Combined effects of alcohol and electrolyte on mass transfer from single carbon-dioxide bubbles in vertical pipes

Hori, Yohei
Hirota, Yutaka
Hayashi, Kosuke
Hosokawa, Shigeo
Tomiyama, Akio

(Citation)
International Journal of Heat and Mass Transfer,136:521-530

(Issue Date)
2019-06

(Resource Type)
journal article

(Version)
Accepted Manuscript

(URL)
https://hdl.handle.net/20.500.14094/90006120

Title: Combined effects of alcohol and electrolyte on mass transfer from single carbon-dioxide bubbles in vertical pipes

Authors: Yohei Hori, Yutaka Hirota, Kosuke Hayashi, Shigeo Hosokawa, Akio Tomiyama*

Affiliation: Graduate School of Engineering, Kobe University

Address: 1-1 Rokkodai, Nada, Kobe, Hyogo 657-8501, Japan

*Corresponding author:

Akio Tomiyama
Professor
Department of Mechanical Engineering
Graduate School of Engineering
Kobe University
Tel. & Fax: +81-78-803-6131
e-mail address: tomiyama@mech.kobe-u.ac.jp

Abstract

Mass transfer rates, k_L, of single carbon-dioxide (CO_2) bubbles rising through vertical pipes filled with alcohol–electrolyte mixed aqueous solutions were measured to investigate the combined effects of alcohol and electrolyte on k_L. 1-octanol and 1-heptanol, which are known to adsorb to the interface and behave like surfactant, were used. Sodium chloride (NaCl) was used for the electrolyte. The surface tension, σ, decreased with increasing the NaCl concentrations, C_N, while keeping the alcohol concentration, C_A, constant. Three combinations of C_A and C_N having the same values of σ were selected for the experimental conditions to avoid the effect of σ. The pipe diameters, D, were 12.5 and 18.2 mm. A wide range of bubble diameter covered various bubble shapes, i.e. ellipsoidal, cap, semi-Taylor and Taylor bubbles. The conclusions obtained are as follows: (1) the combination of C_A and C_N for the same σ does not affect the aspect ratios of ellipsoidal bubbles and the lengths, L, of Taylor bubbles, (2) the Sherwood numbers, Sh, of bubbles in alcohol–NaCl mixed aqueous solutions depend on the combination of C_A and C_N due to the change in the Schmidt number, Sc, even at the same σ for all the tested combinations of concentrations of impurities, and (3) the modified Sherwood number, Sh_D, of contaminated Taylor bubbles is well correlated in terms of the bubble Reynolds number, Sc, the dimensionless group for surfactant properties and L/d_T, where d_T is the transition bubble diameter at the transition from the ellipsoidal–cap bubble regime to the transition regime.

Keywords: Sodium chloride; 1-octanol; Surface tension; Sherwood number

1. Introduction

Mass transfer between bubbles and liquid has been utilized in many industrial systems such as chemical reactors [1], sequestration of carbon dioxide (CO_2) in ocean [2] and so on. The presence of impurities, e.g. surface-active agents (surfactants) and surface-inactive electrolytes, is known to affect the mass transfer rate, k_L. A number of studies have therefore been carried out to make clear the effects of the impurities on k_L.

It is known that alcohols dissolving in the liquid phase accumulate on the gas-liquid interface and behave like surfactant. The adsorption of surfactant reduces the surface tension and the resultant non-uniform distribution of surface tension causes a force tangential to the interface, i.e. the Marangoni force, which decreases the rise velocity [3] and k_L of ellipsoidal bubbles [4]. Koide et al. [4] measured k_L of bubbles in water contaminated with 1-hexanol, 1-heptanol and 1-octanol. The presence of alcohol decreased k_L and the increase in the carbon chain length made the effect stronger. The authors [5] also investigated the effects of carbon chain length on k_L of bubbles in vertical pipes. The k_L of ellipsoidal bubbles decreased with increasing the alcohol concentrations, C_A, whereas they were independent of C_A at high concentrations, i.e. the bubbles were fully-contaminated from the point of view of mass transfer. The k_L of ellipsoidal bubbles fully-contaminated with alcohols decreased with increasing the carbon chain length. The increase in the carbon chain length also decreased k_L of fully-contaminated Taylor bubbles.

The presence of electrolyte is also known to affect the surface tension, i.e. the surface tension increases as the electrolyte concentration increases [6], and to reduce the diffusion coefficients of gaseous species in liquid [7] and the solubility of the gas phase [8]. Baz-Rodriguez et al. [9] and Ruen-ngam et al. [10] carried out experiments on mass transfer in bubbly flows in bubble columns and reported that the presence of electrolyte decreases the net mass transfer rate in bubbly flows. The authors [11] investigated the effects of electrolyte on k_L of single bubbles in vertical pipes using sodium chloride (NaCl) for the electrolyte. Although k_L

of bubbles in the pipes decreased with increasing the NaCl concentration, C_N, mainly due to the reduction of the diffusion coefficient of CO_2 in the liquid phase, the Sherwood numbers, *Sh*, of bubbles in NaCl aqueous solutions were the same as those in clean water.

Yekeen et al. [12] investigated the combined effects of surfactant and electrolyte on the adsorption kinetics and reported that the presence of the electrolyte enhanced the adsorption of surfactant to an interface. Xu et al. [13] measured the surface tension, σ, of aqueous solutions of the 0.05% anionic surfactant, sodium dodecyl sulfate (SDS) for various C_N. Their results showed that σ in the presence of electrolyte decreases with increasing C_N. They pointed out that the reduction in σ is due to the increase in the surfactant concentration at the interface caused by the binding of Na^+ ions to SDS^- ions, resulting in the reduction of the repulsion between SDS^- ions. Although the combined effects of electrolyte and surfactant on σ have been investigated, studies on the combined effects on k_L have rarely been reported.

Combined effects of surfactant and electrolyte on k_L of single CO_2 bubbles in vertical pipes were, therefore, investigated in this study. NaCl and 1-octanol were used for the electrolyte and the surfactant, respectively. The pipe diameters, *D*, were 12.5 and 18.2 mm. The diameter ratio, λ, which is the ratio of the sphere-volume-equivalent bubble diameter, *d*, to *D* was widely varied to cover various bubble shapes such as ellipsoidal, cap, semi-Taylor and Taylor bubbles.

2. Experimental

Fig. 1 shows the experimental setup, which consists of the vertical pipe, the lower and upper tanks and the reservoir. The upper tank and the reservoir were open to the atmosphere, and therefore, the gas components in the liquid were in their equilibrium to the atmosphere. Two pipes of D = 12.5 and 18.2 mm were used. The pipe length was 2000 mm. The reference elevation (z = 0 mm) was set at 1900 mm below the free surface of the liquid in the upper tank. The pipe was made of fluorinated-ethylene-propylene (FEP) resin, whose refractive index is close to that of water, i.e. the refractive indexes of FEP resin and water are 1.338 and 1.333, respectively. The FEP pipe was installed in the acrylic duct. Water was filled in the gap between the duct and the pipe to reduce optical distortion in bubble images. Water purified using a Millipore system (Elix 3) and CO_2 of 99.9 vol.% purity were used for the liquid and gas phases, respectively. NaCl (99.5% purity, Wako Pure Chemical Industries) and 1-octanol (98.0% purity, Wako Pure Chemical Industries) were used for the electrolyte and the surfactant, respectively. The sorption properties of the 1-octanol [14] in the following Langmuir isotherm [15] are summarized in **Table 1**:

$$j = k_a C_A(\Gamma_m - \Gamma) - k_d\Gamma \tag{1}$$

where j is the net adsorption flux of surfactant between the bulk liquid phase and the interface, k_a the adsorption rate constant, k_d the desorption rate constant, Γ the interfacial surfactant concentration, and Γ_m the saturated interfacial surfactant concentration.

Fig. 2 shows σ of 1-octanol–NaCl mixed aqueous solutions (triangle and square symbols). The σ decreases with increasing C_N for each C_A condition (C_A = 0.17 and 0.30 mol/m^3) and reaches the value of 1-octanol aqueous solution of C_A = 0.77 mol/m^3 (circle symbol). The decrease in σ implies that the alcohol concentration at interface increases with C_N. Therefore the presence of NaCl enhances the adsorption of 1-octanol. The three combinations of C_N and C_A having the same values of σ were used in the following experiments on bubbles to investigate the combined effects on k_L of bubbles. The fluid properties in the three conditions

are given in **Table 2**, where ρ_L is the liquid density, and μ_L the liquid viscosity. The diffusion coefficients, D_L, of CO_2 in NaCl aqueous solutions [7] were 1.90×10^{-9}, 1.66×10^{-9} and 1.50×10^{-9} m^2/s at C_N = 0, 8.5 and 14 wt.%, respectively. Note that the data at C_A = 0.77 mol/m^3 and C_N = 0 wt.%, at which bubbles were confirmed to be fully-contaminated from the point of view of k_L, were quoted from our previous paper [17].

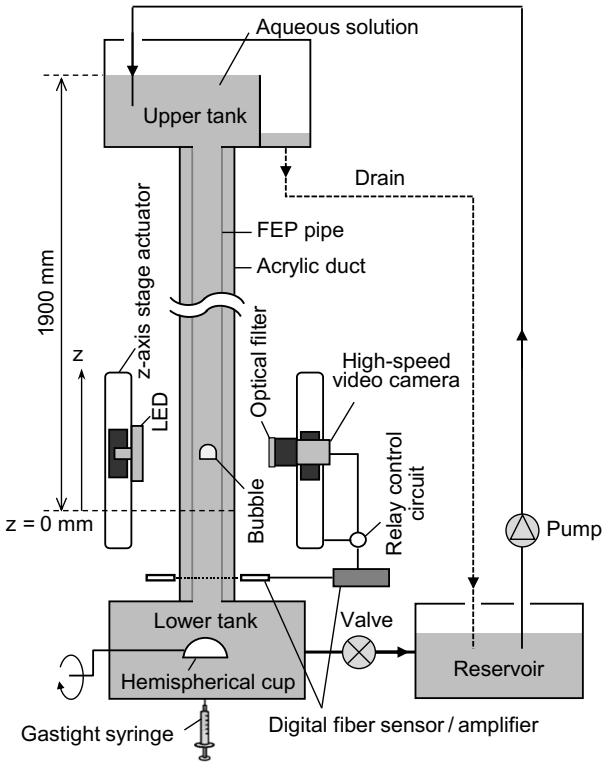

Fig. 1 Experimental setup

Table 1 Sorption properties of alcohols [14,16]

Alcohol	k_a [m^3/mol s]	k_d [1/s]	Γ_m [mol/m^2]
1-octanol	170	68	7.5×10^{-6}
1-heptanol	100	110	6.0×10^{-6}

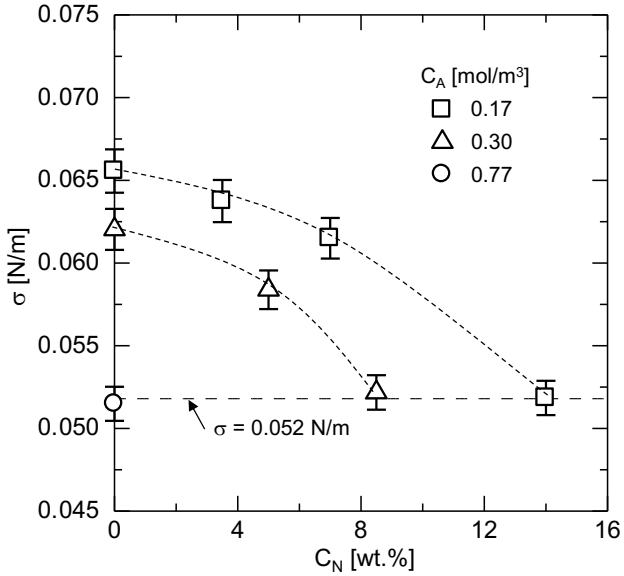

Fig. 2 Surface tension of interface between air and 1-octanol–NaCl mixed aqueous solution

Table 2 Physical properties of 1-octanol−NaCl mixed aqueous solution

C_A [mol/m^3]	C_N [wt.%]	σ [N/m]	ρ_L [kg/m^3]	μ_L [Pa·s]
0.77	0	0.051	997	0.89×10^{-3}
0.30	8.5	0.052	1057	1.03×10^{-3}
0.17	14.0	0.052	1095	1.17×10^{-3}

Measurements of k_L were carried out for bubbles rising through the stagnant liquids in the pipes at atmospheric pressure and room temperature (298 ± 1.0 K). The liquid in the pipe was refreshed before each run by circulating the liquid using the pump to make the dissolved CO_2 concentration negligibly small as shown in **Fig. 1**. A predetermined amount of CO_2 gas, whose volume was measured by using the gastight syringe, was injected from the bottom of the lower tank and stored in the hemispherical cup. A single bubble was released by rotating the cup. Front and side images of a bubble in the test section were recorded using the two synchronized video cameras (Integrated Design Tool, M3, frame rate: 250 frame/s, exposure time: 1000 μs, spatial resolution: 0.04–0.05 mm/pixel), which were mounted on the *z*-axis actuators (SUS Corp., SA-S6AM). The green and red LED light sources (NICHIA, NSPG510AS; ROHM, SLI-580UT3F) were used for back illumination. The motion of the cameras and the LED lights were synchronized using the actuators. Bubbles were tracked for $0 \leq z \leq 550$ mm. An image

processing method [18] was utilized to measure bubble volumes, diameters and positions. The original gray-scale images were transformed into binary images. By assuming that the horizontal cross sections of a bubble were elliptical, a three dimensional bubble shape was reconstructed by piling up the elliptic disks. The sphere-volume-equivalent bubble diameters, d, were evaluated from the volume of the reconstructed bubble shapes. The bubble rise velocities, V_B, were calculated from the rates of change in the axial bubble position. Uncertainties estimated at 95% confidence in d and V_B were ± 2.1% and 0.20%, respectively. The d ranged from 5 to 25 mm, and therefore, the ranges of the diameter ratio, λ (= d/D), were 0.4–1.7 and 0.3–1.4 for D = 12.5 and 18.2 mm, respectively.

The k_L and Sh were evaluated from the rate of decrease in d [18]. **Fig. 3** shows an example of time evolutions of d in the pipe of D = 12.5 mm. When a flow is isothermal, the change in the moles, n, of CO_2 inside a bubble is given by

$$\frac{\mathrm{d}n}{\mathrm{d}t} = -k_L A(C_S - C_0) \tag{2}$$

where t is the time, A (= πd^2) the bubble surface area, Cs the CO_2 concentrations at the bubble surface [8], and C_0 the CO_2 concentration in the liquid phase. Assuming C_S is given by Henry's law and $C_0 << C_S$ yield

$$k_L = -\frac{1}{\pi d^2}\frac{H - P(z)X}{C_L P(z)X}\frac{\mathrm{d}n}{\mathrm{d}t} \tag{3}$$

where H is the Henry constant, X the mole fraction of CO_2 in a bubble, C_L the H_2O concentration (55.4 kmol/m^3), and P the pressure inside a bubble given by

$$P(z) = P_{atm} + \rho_L g\, h\,(z) \tag{4}$$

where P_{atm} is the atmospheric pressure, g the acceleration of gravity, and $h(z)$ the distance from the free surface to the bubble center. The X in Eq. (3) was assumed to be unity, since a bubble arrived at the test section within 15 s after the injection of CO_2 gas into the hemispherical cup so that the change in the gas composition inside the bubble was negligibly small (see Appendix

A1). By assuming that CO_2 is an ideal gas, dn/dt can be expressed in terms of P and d as follows:

$$\frac{\mathrm{d}n}{\mathrm{d}t} = \frac{\pi}{6RT}\frac{\mathrm{d}(Pd^3)}{\mathrm{d}t} \tag{5}$$

where R is the universal gas constant. The k_L was calculated by substituting Eq. (5) into Eq. (3) and evaluating d(Pd^3)/dt by using the centered difference between t_1 and t_2:

$$k_L = \frac{(H - P_{12})(P_2 d_2^3 - P_1 d_1^3)}{6RT(t_2 - t_1)d_{12}^2 C_L P_{12}} \tag{6}$$

where the subscripts, 1, 2 and 12, represent the times, t_1, t_2 ($> t_1$) and t_{12} ($= (t_1 + t_2)/2$), respectively. The bubble diameters at t_1, t_2 and t_{12} were obtained from a linear regression equation fitted to the measured d (**Fig. 3**). The Sh defined by

$$Sh = \frac{k_L d}{D_L} \tag{7}$$

was calculated from k_L by using d_{12} for d.

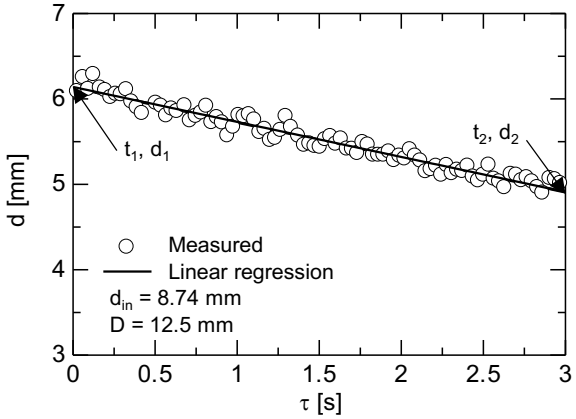

Fig. 3 Measured diameter of a CO_2 bubble (d_{in} is the initial bubble diameter)

3. Results and discussion

3.1 Bubble shape and velocity

Fig. 4 shows examples of the images of a clean ellipsoidal bubble **(a)** and contaminated ellipsoidal bubbles, i.e. bubbles in 1-octanol aqueous solution **(b)** and in 1-octanol–NaCl mixed aqueous solutions **(c and d)**. They showed wobbling motion. The effect of the presence of 1-octanol on the bubble shape is clearly seen in the figure, i.e. capillary waves are formed at the interface of the clean ellipsoidal bubble but not at those of the contaminated ellipsoidal bubbles.

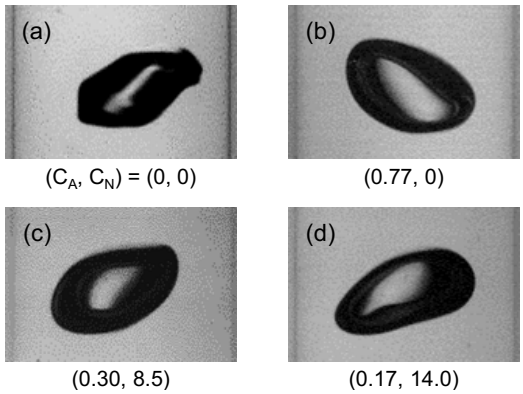

Fig. 4 Shapes of ellipsoidal bubbles (d = 6 mm)

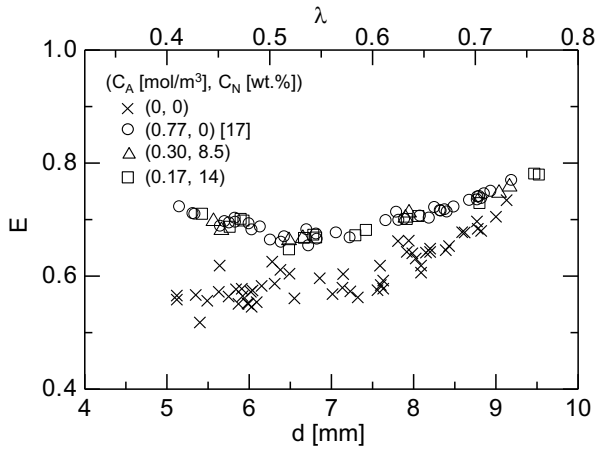

Fig. 5 Aspect ratios of ellipsoidal bubbles (D =12.5 mm)

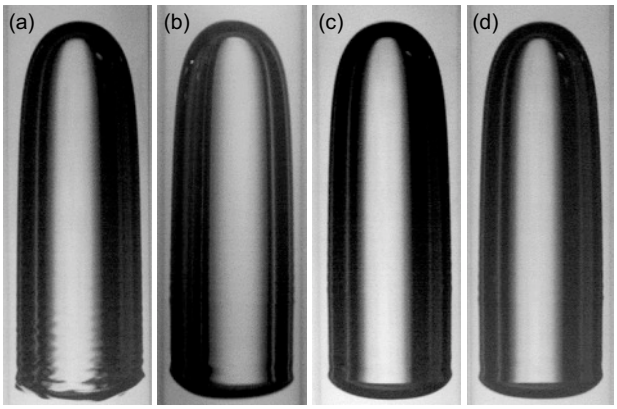

Fig. 6 Shapes of Taylor bubbles (λ = 1.5, d = 16 mm)

Fig. 5 shows the time-averaged aspect ratios, E (= d_V/d_H), of the ellipsoidal bubbles at D = 12.5 mm, where d_V and d_H are the maximum vertical dimension and the maximum horizontal dimension of a bubble, respectively. The E of bubbles in 1-octanol–NaCl mixed aqueous solutions are almost the same as those of bubbles in the fully-contaminated 1-octanol aqueous solutions. In spite of the differences in C_A and C_N, E are almost the same in all the conditions because of the same σ. In all the cases, E increases with increasing d for $\lambda > 0.55$. This is due to the effect of the pipe wall. **Fig. 6** shows examples of the clean and contaminated Taylor bubbles (λ = 1.5, D = 12.5 mm). Capillary waves are formed in the tail region of the clean Taylor bubbles, whereas they are attenuated by the presence of impurities. It should be noted that the shape oscillation due to the capillary waves rarely affects the total mass transfer from Taylor bubbles [19]. **Fig. 7** shows the lengths, L, of the Taylor bubbles (the axial distance between the nose and the tail). The L strongly depend on D, while the effects of C_N and C_A are negligibly small. The ratios of L to D are shown in **Fig. 8**. The following L/D correlation for clean Taylor bubbles proposed by Nakahara et al. [20] is also shown in the figure.

$$\frac{L}{D} = (0.586 - 0.216\lambda + 0.844\lambda^2)\lambda \tag{9}$$

Eq. (9) can well evaluate L/D of contaminated Taylor bubbles in all the cases.

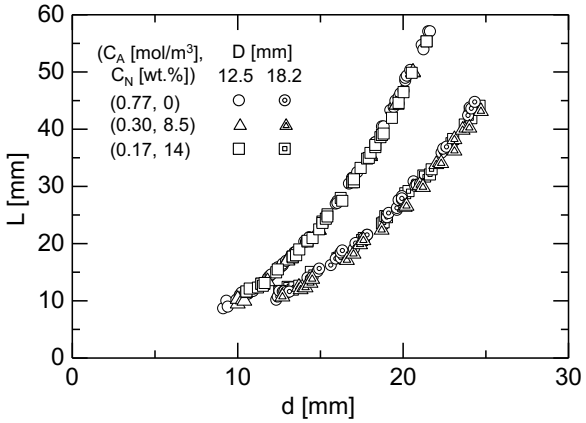

Fig. 7 Lengths of contaminated Taylor bubbles

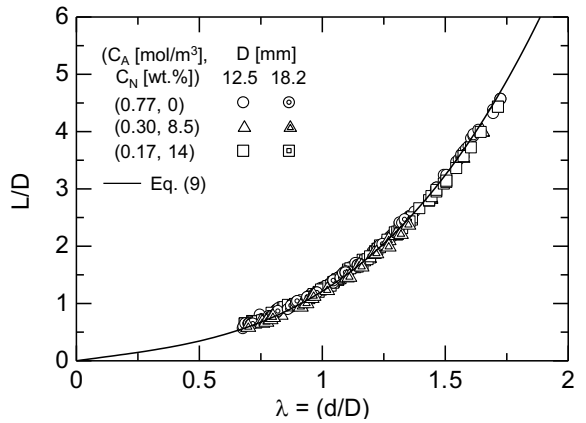

Fig. 8 Comparisons of measured L/D with Eq. (9)

The V_B are shown in **Fig. 9**, in which the data are classified into three regimes, the ellipsoidal-cap bubble regime, the transition (semi-Taylor bubble) regime, and the Taylor bubble regime. The d_T in the figure is the bubble diameter at the transition from the ellipsoidal-cap bubble regime to the transition regime (d_T = 9.7 and 12.2 mm for D = 12.5 and 18.2 mm, respectively) [11], which was defined as the bubble diameter at the abrupt change in the trend of V_B. The Taylor bubble regime can be clearly identified since V_B is independent of d. The V_B in the ellipsoidal-cap bubble regime decreases with increasing d. The V_B in the transition regime, in which the characteristic length governing V_B changes from d to D, shows complex dependence on d. The decrease in V_B due to the presence of impurities is clearly seen for $\lambda < 0.55$ and can be attributed to the Marangoni effect [3]. The effects of C_N and C_A on V_B of contaminated ellipsoidal bubbles are small for $\lambda > 0.55$ since the inertial force is dominant in the bubble motion in this range.

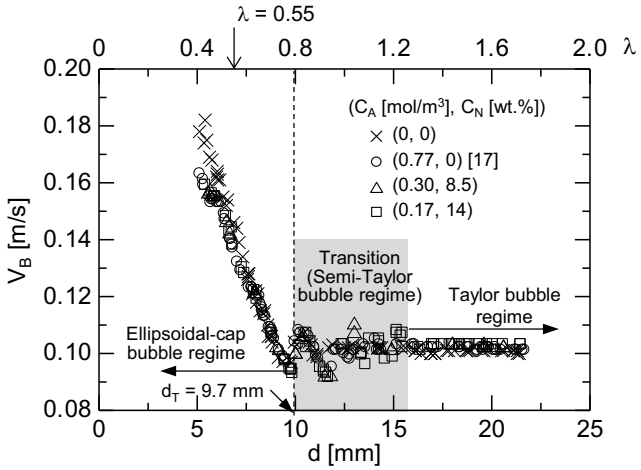

(a) D = 12.5 mm

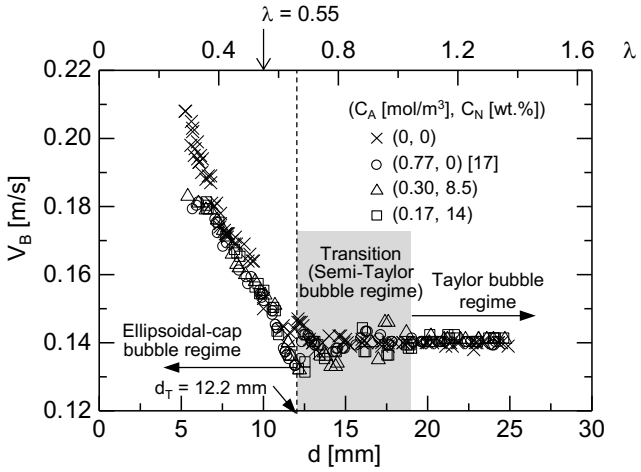

(b) D = 18.2 mm

Fig. 9 Bubble rise velocities

3.2 Mass transfer rate and Sherwood number

Fig. 10 shows k_L of clean and contaminated bubbles. Since the bubble lateral motion in the ellipsoidal regime became stronger with increasing D, the scatter in the data of D = 18.2 mm was larger than that of D = 12.5 mm (see Appendix A2). The k_L of contaminated ellipsoidal bubbles were much lower than those of clean bubbles whereas k_L of contaminated Taylor bubbles increase with d and approach those of clean bubbles. Although the trend of k_L changes at d larger than d_T, i.e. $d \approx$ 11.7 and 14 mm at D = 12.5 and 18.2 mm, respectively, The bubble diameter, $d^* = d/d_T$, scaled with d_T can be used in correlating k_L and the change in the trend of k_L takes place at $d^* \approx$ 1.2 as discussed in the following.

In **Fig. 11** *Sh* are plotted against the bubble Reynolds number *Re* defined by

$$Re = \frac{\rho_L V_B d}{\mu_L} \tag{10}$$

The *Sh* increases with increasing *Re* and the combination of C_N and C_A affects *Sh*. It is well known that *Sh* of contaminated spherical bubbles with immobile interface is well correlated in terms of $Re^{1/2}Sc^{1/3}$ [21], and in our previous studies [5,17] we confirmed that this factor is also applicable to bubbles fully-contaminated with alcohol, where S_C is the Schmidt number defined by

$$Sc = \frac{\mu_L}{\rho_L D_L} \tag{11}$$

Hence *Sh* are plotted against $Re^{1/2}Sc^{1/3}$ in **Fig. 12**, where *Sc* = 470, 590 and 710 for C_N = 0, 8.5 and 14 wt.%, respectively. The present data are also well correlated using $Re^{1/2}Sc^{1/3}$, implying that bubbles were fully-contaminated even at C_A = 0.17 and 0.30 mol/m^3 due to the adsorption enhancement effect by NaCl.

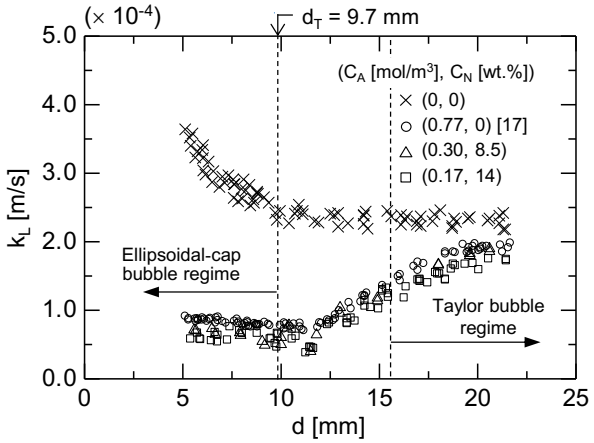

(a) *D* = 12.5 mm

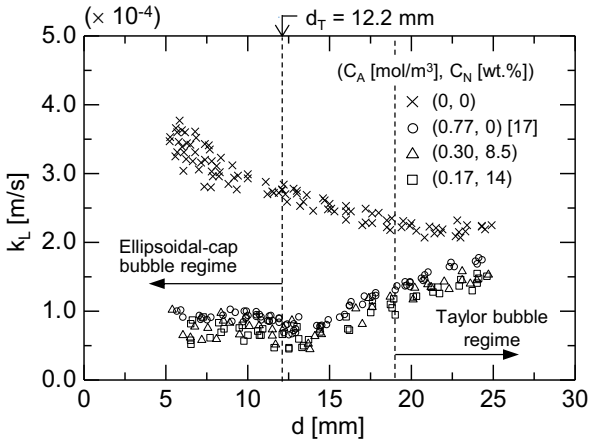

(b) *D* = 18.2 mm

Fig. 10 Mass transfer rates

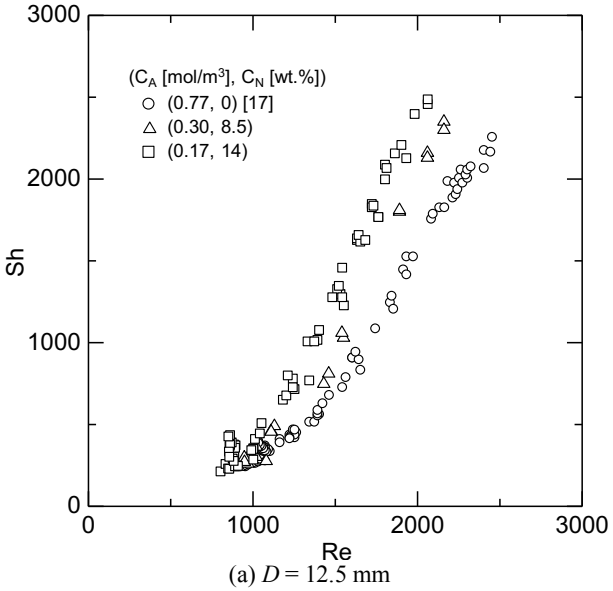

(a) D = 12.5 mm

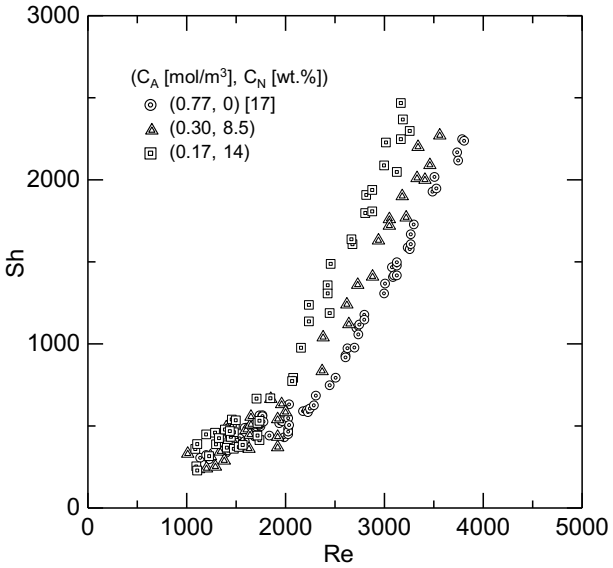

(b) D = 18.2 mm

Fig. 11 Sherwood numbers

Fig. 13 shows a comparison between the data and the following *Sh* correlation for bubbles fully-contaminated with 1-octanol proposed in our previous study [17]:

$$Sh = F(d^*)Re^{1/2}Sc^{1/3} \tag{12}$$

$$F(d^*) = \begin{cases} 0.47d^{*2} + 0.47d^* + 0.6 & \text{for Ellipsoidal-cap bubbles} \\ -0.86d^{*2} + 7.0d^* - 5.8 & \text{for Taylor bubbles} \end{cases} \tag{13}$$

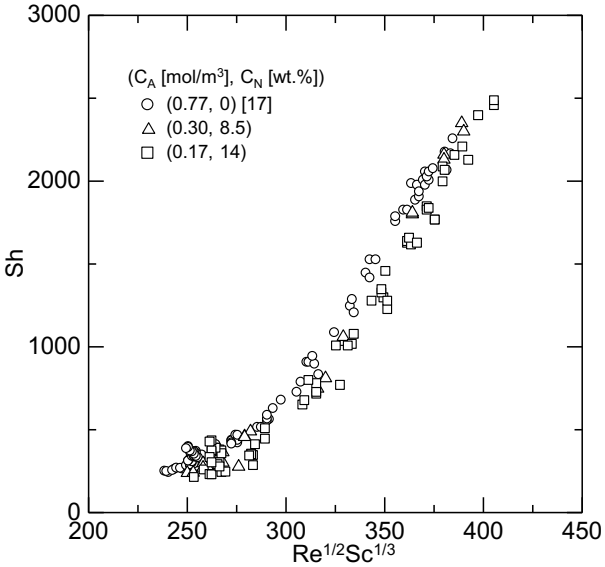

(a) D = 12.5 mm

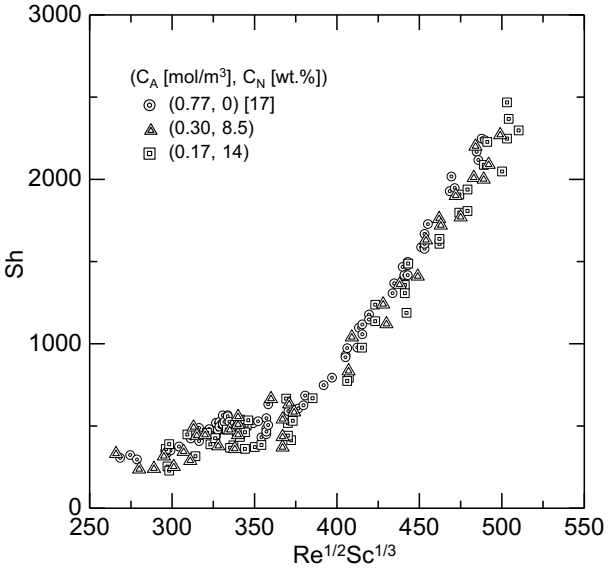

(b) D = 18.2 mm

Fig. 12 *Sh* vs. $Re^{1/2}Sc^{1/3}$

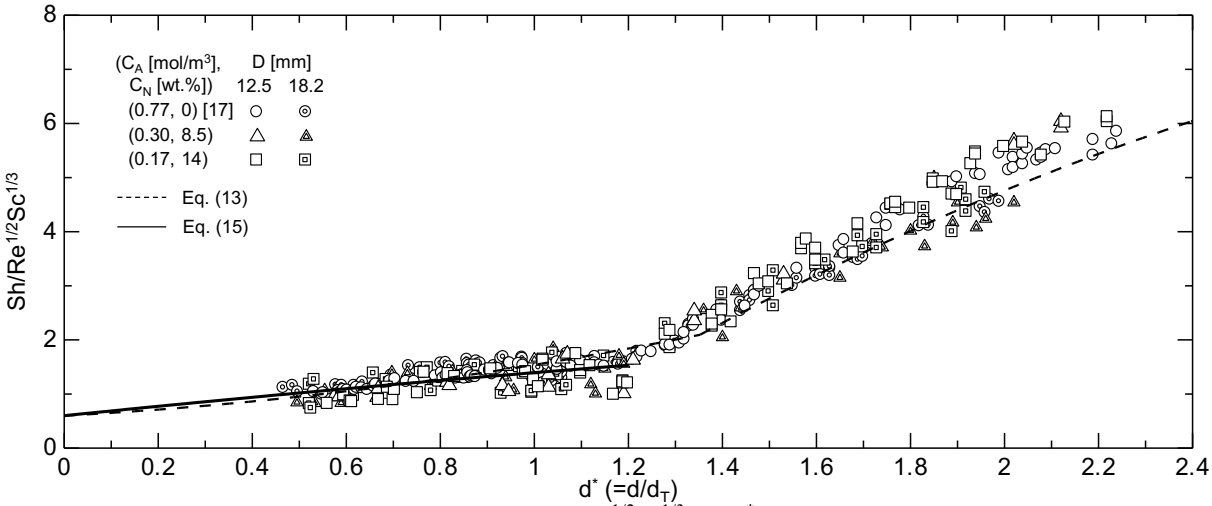

Fig. 13 $Sh/Re^{1/2}Sc^{1/3}$ vs. d^*

where d^* is the dimensionless bubble diameter defined by

$$d^* = d / d_T \tag{14}$$

Eq. (12) can evaluate 81% and 53% of the data within ± 20% and ± 10% errors, respectively as shown in **Fig. 14(a)**. Since Eq. (12) was not recommended for the transition regime [17], Eq. (12) tends to overrate the data in the transition regime. The coefficients in $F(d^*)$ for $d^* \leq 1.2$ are therefore modified as

$$F(d^*) = -0.10d^{*2} + 0.88d^* + 0.6 \tag{15}$$

Eq. (15) is shown in the **Fig. 13** as the solid line. **Fig. 14(b)** compares Eq. (12), in which F were evaluated using Eq. (15), with the data. The agreements are better than those using Eq. (13), i.e. 85% and 62% of the data lie to within ± 20% and ± 10% errors, respectively. For $d^* > 1.2$, Eq. (12) tends to underestimate Sh at D = 12.5 mm as shown in **Figs. 13 and 15**. Therefore Eq. (12) cannot appropriately account for the effects of D on Sh of Taylor bubbles.

Filla [22] proposed the following Sherwood number correlation for clean Taylor bubbles of $L/D > 1$:

$$Sh_D = 5.1\left(\frac{L}{D}\right)^{0.8} Re_D^{1/2} Sc^{1/2} \tag{16}$$

where Sh_D and Re_D are the modified Sherwood number and the modified bubble Reynolds number defined by

$$Sh_D = \frac{k_L A}{D_L D} \tag{17}$$

and

$$Re_D = \frac{\rho_L V_B D}{\mu_L} \tag{18}$$

respectively. The data of $Sh_D/Re_D^{1/2}Sc^{1/3}$ are plotted against L/D in **Fig. 16**. The data show two

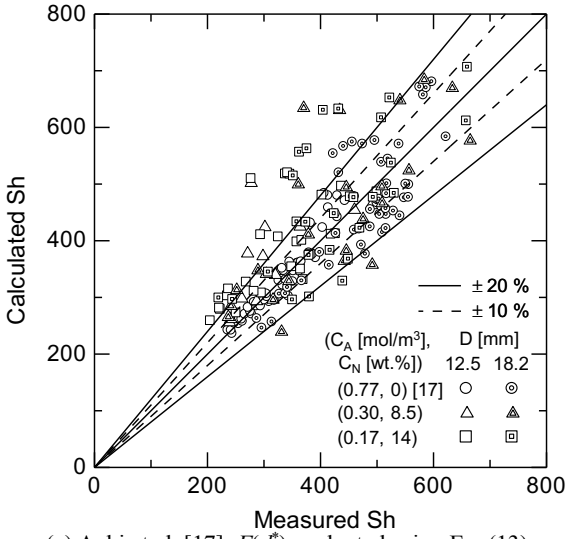

(a) Aoki et al. [17]: $F(d^*)$ evaluated using Eq. (13).

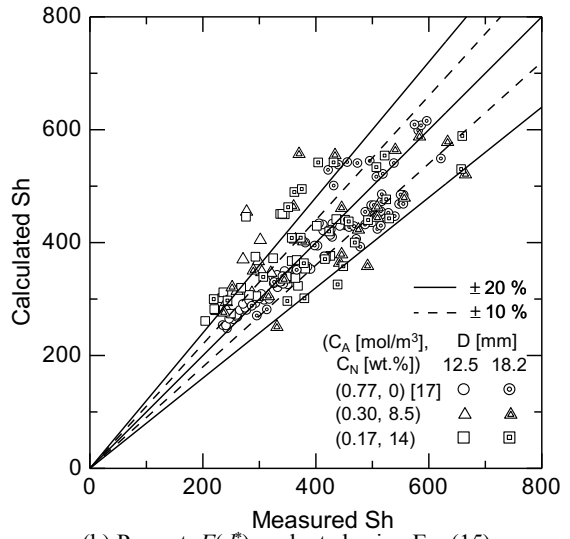

(b) Present: $F(d^*)$ evaluated using Eq. (15).

Fig. 14 Comparisons between Eq. (12) and data for $d^* \leq 1.2$

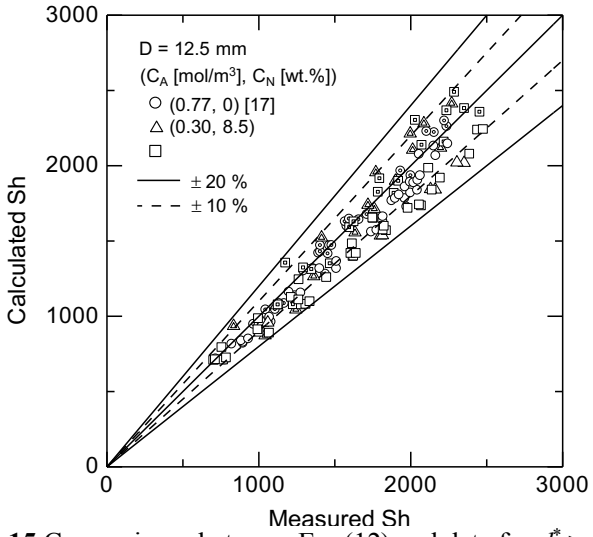

Fig. 15 Comparisons between Eq. (12) and data for $d^* > 1.2$. The $F(d^*)$ in Eq. (12) were evaluated using Eq. (13).

curves depending on D. In our previous studies, we confirmed that the effects of D can be implicitly well taken into account by using the transition bubble diameter d_T [5,11,17], since the regime transition from the ellipsoidal-cap bubble regime to the transition regime takes place at $d = d_T$. The Sh_D for Taylor bubbles can therefore be given by

$$Sh_D = G(L / d_T)Re_D^{1/2}Sc^{1/3} \tag{19}$$

where G is a function of L/d_T. The $Sh_D/Re_D^{1/2}Sc^{1/3}$ are plotted against L/d_T in **Fig. 17(a)**. The data are collapsed onto a single curve. The effect of D, therefore, can be implicitly well taken into account in Sh correlations by using L/d_T.

Since the carbon chain length of alcohol affects k_L, the applicability of the functional form of Eq. (19) to an alcohol of different carbon chain length, i.e. 1-heptanol (98.0% purity, Wako Pure Chemical Industries), was also examined. The surfactant properties of 1-heptanol [16] and the experimental conditions are summarized in **Tables 1** and **3**, respectively. The σ of 1-heptanol–NaCl mixed aqueous solutions also decreased with increasing C_N while keeping C_A constant. The data of $Sh_D/Re_D^{1/2}Sc^{1/3}$ in 1-heptanol–NaCl mixed aqueous solutions are well correlated in terms of L/d_T as shown in **Fig. 17(b)**. However **Figs. 17 (a) and (b)** imply that the function G depends not only on L/d_T, but also on the surfactant properties.

Since the surfactant properties depend on the carbon chain length and they are characterized by k_a, k_d and Γ_m, the authors [5] introduced the following dimensionless group, θ, to take into account the effect of the carbon chain length of alcohol on k_L of bubbles in alcohol aqueous solutions:

$$\theta = \frac{k_a \Gamma_m}{k_d d_T} \tag{20}$$

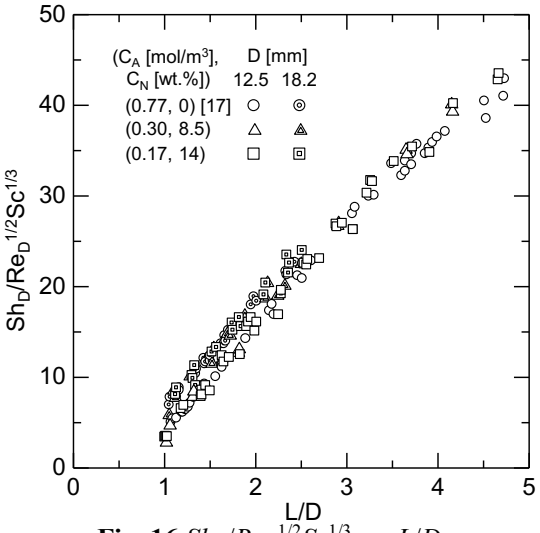

Fig. 16 $Sh_D/Re_D^{1/2}Sc^{1/3}$ vs. L/D

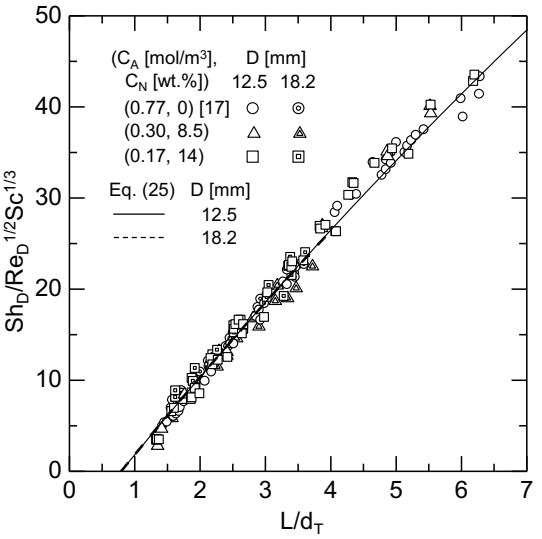

(a) 1-octanol–NaCl mixed aqueous solutions

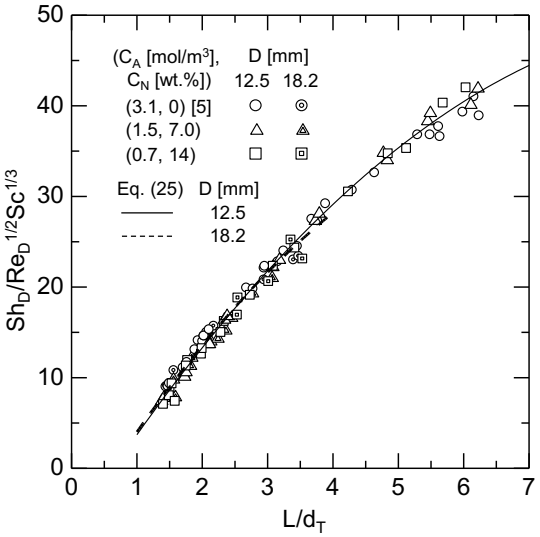

(b) 1-heptanol–NaCl mixed aqueous solutions

Fig. 17 $Sh_D/Re_D^{1/2}Sc^{1/3}$ vs. L/d_T

Table 3 Physical properties of 1-heptanol–NaCl mixed aqueous solutions

C_A [mol/m^3]	C_N [wt.%]	σ [N/m]	ρ_L [kg/m^3]	μ_L [Pa·s]
3.1	0	0.051	997	0.89×10^{-3}
1.5	7.0	0.052	1051	1.00×10^{-3}
0.7	14.0	0.051	1095	1.17×10^{-3}

This dimensionless group can also be express as a combination of typical dimensionless groups, i.e.

$$\theta = LaK\frac{L}{d_T} \tag{21}$$

where *La* and *K* are the Langmuir number and the dimensionless adsorption length defined by

$$La = \frac{k_a C_A}{k_d} \tag{22}$$

and

$$K = \frac{\Gamma_m}{C_A L} \tag{23}$$

respectively. Eq. (19) can therefore be extended as

$$Sh_D = G(L/d_T, \theta) Re_D^{1/2} Sc^{1/3} \tag{24}$$

Expressing G as a quadratic function, $G = A(\theta)(L/d_T)^2 + B(\theta)(L/d_T) + C$, and fitting this equation to the data yield

$$C = -7.0 \tag{25}$$

and $A(\theta)$ and $B(\theta)$ shown in **Fig. 18**. The following correlations well fit the data:

$$A(\theta) = -5.6 \times 10^{-5} \theta^{-1.2} \tag{26}$$

$$B(\theta) = 2.8\theta^{-0.19} \tag{27}$$

Thus

$$Sh_D = \left[A(\theta)(L/d_T)^2 + B(\theta)(L/d_T) + C \right] Re_D^{1/2} Sc^{1/3} \tag{28}$$

Eqs. (25)–(28) give reasonable evaluations of Sh_D of Taylor bubbles contaminated with alcohol as shown in **Fig. 17**. Comparisons between Eq. (25) and the measured data are shown in **Fig. 19**.

98% and 89% of the data are to within ± 20% and ± 10% errors, respectively. The agreements are much better than Eq. (12). Therefore the present way to correlate the Sherwood numbers in terms of L/d_T, θ and $Re_D^{1/2}Sc^{1/3}$ would be of use in developing *Sh* correlations for alcohol–electrolyte mixed aqueous solutions.

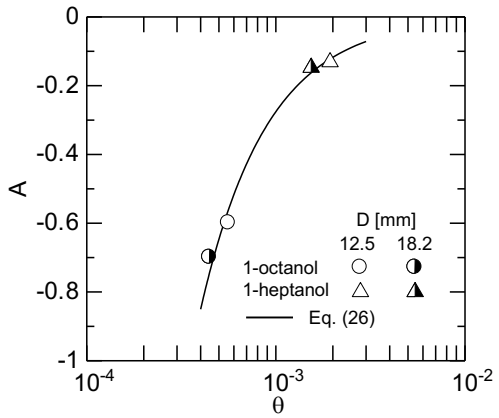

(a) $A(\theta)$

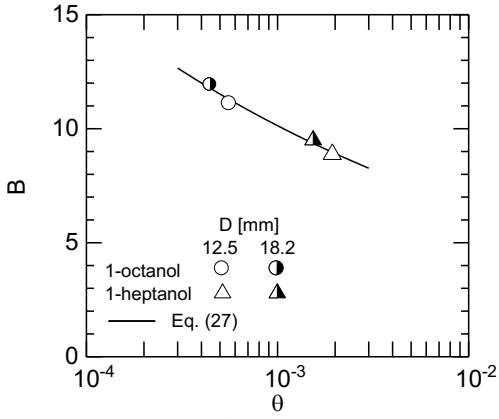

(b) $B(\theta)$

Fig. 18 *A* and *B* vs. θ

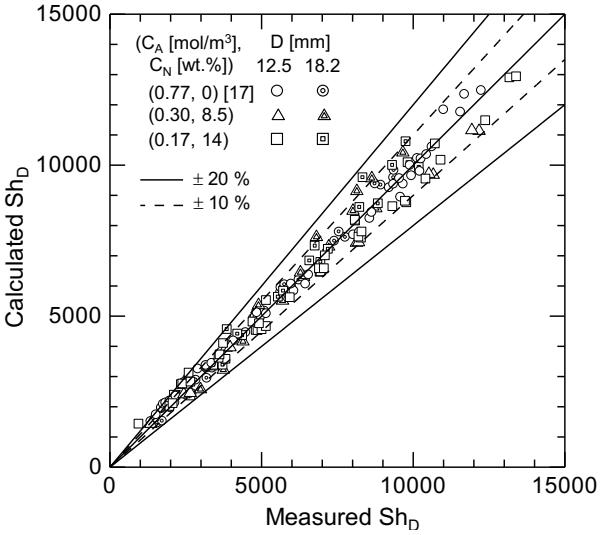

(a) 1-octanol–NaCl mixed aqueous solutions

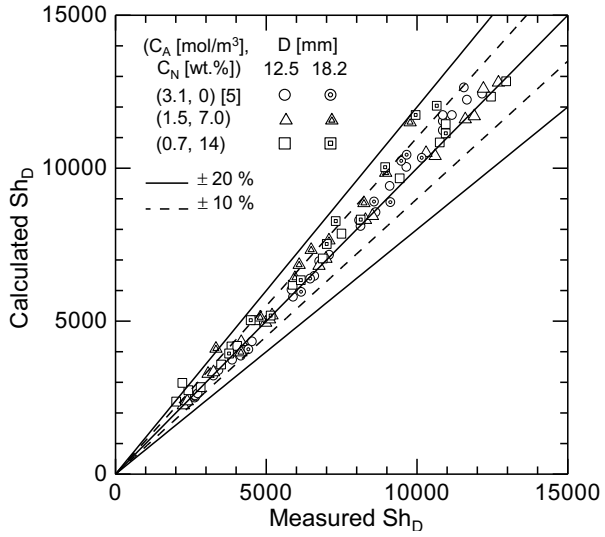

(b) 1-heptanol–NaCl mixed aqueous solutions

Fig. 19 Comparisons between Eq. (25) and data

4. Conclusions

Combined effects of alcohol and NaCl on mass transfer from single carbon-dioxide bubbles rising through vertical pipes were investigated. Two alcohols, i.e.1-octanol and 1-heptanol, were used for the alcohol. Sodium chloride (NaCl) was used for the electrolyte. Three combinations of the alcohol concentrations, C_A, and the NaCl concentrations, C_N, having the same values of surface tension, σ, were selected for the experimental conditions to avoid the effect of σ. The pipe diameters, D, were 12.5 and 18.2 mm. The bubble diameter, d, was varied to cover from ellipsoidal to Taylor bubbles. The mass transfer rates, k_L, were evaluated from the rate of change in d and the Sherwood numbers, Sh, were calculated from k_L. The following conclusions were obtained:

(1) The combination of C_A and C_N for the same σ does not affect the aspect ratios of ellipsoidal bubbles and the length, L, of Taylor bubbles.

(2) The Sh of bubbles in alcohol–NaCl mixed aqueous solutions depend on the combination of C_A and C_N due to the change in the Schmidt number, Sc, even at the same σ for all the combinations of concentrations of impurities.

(3) The modified Sherwood number, Sh_D, of contaminated Taylor bubbles is well correlated in terms of the bubble Reynolds number, Sc, the dimensionless group for surfactant properties defined by Eq. (20) and L/d_T, where d_T is the transition bubble diameter at the transition from the ellipsoidal–cap bubble regime to the transition regime.

Acknowledgment

This work has been support by JSPS KAKENHI Grant Number 18H03756.

Appendix A

A.1. Time evolution of mole fractions of CO_2

Fig. A1 shows time evolution of X in bubbles in the 1-octanol–NaCl mixed aqueous solutions predicted using Eqs. (25)–(28), where t is the time elapsed from the injection of a bubble into the lower tank, and d_{in} the initial bubble diameter. Although the decreasing ratios of X in the bubbles of d_{in} = 9.8 mm are larger than those of d_{in} = 26.7 mm, those in the initial several ten seconds are not large in all the cases and they are smaller than 2.0% at t = 15 s. In the measurement of k_L, bubbles reached the measurement section at least within 15 s. This result proves the validity of assuming X = 1 in Eq. (3).

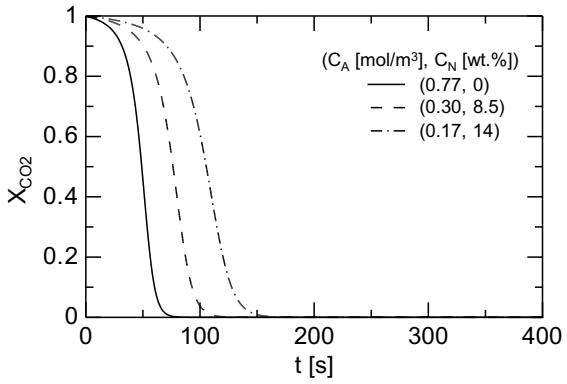

(a) d_{in} = 9.8 mm

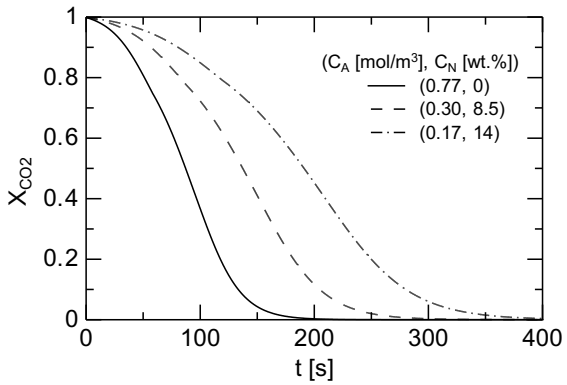

(b) d_{in} = 26.7 mm

Fig. A1 Predicted time evolution of mole fractions of CO_2

A.2 Lateral positions of ellipsoidal bubbles

Fig. A2 shows examples of the trajectories of the ellipsoidal bubbles of d = 6 mm, in which x and y are the horizontal coordinates having their origin at the pipe axis. The fluctuation of the contaminated bubble in the pipe of D = 12.5 mm (b) are smaller than that of clean bubble (a) since the shape oscillation of the contaminated bubble is smaller than that of clean bubble. The bubble fluctuation in D = 18.2 mm (c) is much larger than that in the smaller pipe due to weaker wall effect. The standard deviations, s, of the bubble lateral position, r (= $\sqrt{x^2 + y^2}$), evaluated by

$$s = \sqrt{\frac{1}{N-1}\sum_{i=1}^{N}(r_i - \bar{r})^2} \tag{8}$$

were 1.8, 1.3 and 2.5 mm for **Fig. A2 (a), (b) and (c)**, respectively, where N (= 500) is the total sampling number and the subscript i denotes the segmental number of the images.

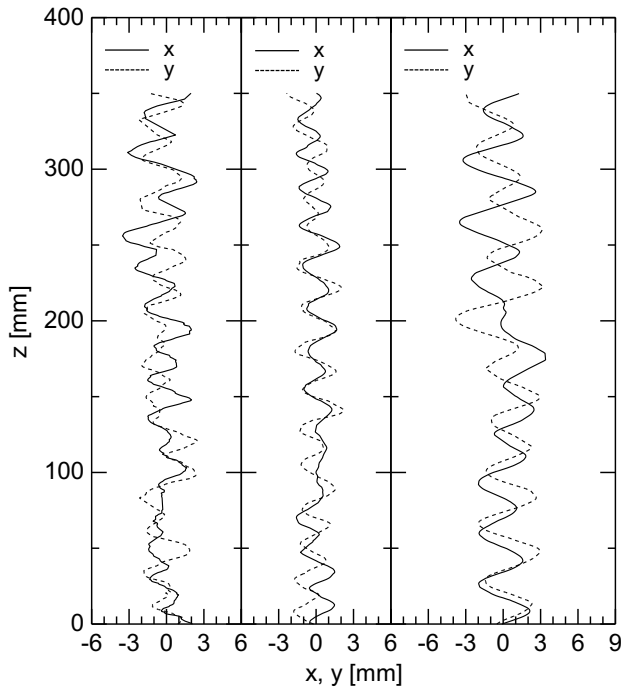

(a) D = 12.5 mm (C_A, C_N) = (0, 0) (b) D = 12.5 mm (0.17, 14) (c) D = 18.2 mm (0.17, 14)

Fig. A2 Lateral positions of ellipsoidal bubbles (d = 6 mm)

References

[1] K. Akita, F. Yoshida, Gas holdup and volumetric mass transfer coefficient in bubble columns, Ind. Eng. Chem. Process Des. Develop. 12 (1973) 76–80.

[2] T. Kajishima, T. Saito, R. Nagaosa, S. Kosugi, GLAD: a gas-lift method for CO_2 disposal into the ocean, Energy, 22 (1997) 257–262.

[3] R. Kurimoto, K. Hayashi, A. Tomiyama, Terminal velocities of clean and fully-contaminated drops in vertical pipes, Int. J. Multiphase Flow 49 (2013) 8–23.

[4] K. Koide, T. Hayashi, K. Sumino, S. Iwamoto, Mass transfer from single bubbles in aqueous solutions of surfactants, Chem. Eng. Sci. 31 (1976) 471–484.

[5] J. Aoki, Y. Hori, K. Hayashi, S. Hosokawa, A. Tomiyama, Mass transfer from single carbon dioxide bubbles in alcohol aqueous solutions in vertical pipes, Int. J. Heat Mass Transfer, 108 (2017) 1991–2001.

[6] P.K. Weissenborn, R.J. Pugh, Surface tension of aqueous solutions of electrolytes: relationship with ion hydrogen, oxygen solubility, and bubble coalescence, J. Col. Interface Sci. 184 (1996) 550–563.

[7] D.M. Himmelblau, Diffusion of dissolved gases in liquid, Chem. Rev. 64 (1964) 527–545.

[8] D.W. van Krevelen, P.J. Hoftijzer, Sur la solubilite des gaz dans les solutions aqueouses, Ind. 21st Congr. Int. Chim. Ind. (1948) 168.

[9] S.A. Baz-Rodriguez, J.E. Botello-Alvarez, A. Estrada- Baltazar. L.E. Vilchiz-Bravo, L.A. Padilla-Medina, R. Miranda-Lopez, Effect of electrolytes in aqueous solutions on oxygen transfer in gas-liquid bubble column, Chem. Eng. Res. Des. 92 (2014) 2352–2360.

[10] D. Ruen-ngam, P. Wongsuchoto, A. Limpanuphap, T. Charinpanitkul, P. Pavasant, Influence of salinity on bubble size distribution and gas-liquid mass transfer in airlift contactors, Chem. Eng. J. 141 (2008) 222–232.

[11] Y. Hori, K. Hayashi, S. Hosokawa, A. Tomiyama, Mass transfer from single carbon-dioxide bubbles in electrolyte aqueous solutions in vertical pipes, Int. J. Heat Mass Transfer, 111 (2017) 663–671.

[12] N. Yekeen, M. A. Manan, A. K. Idris, A. M Samin, Influence of surfactant and electrolyte concentrations on surfactant adsorption and foaming characteristics, J. Petro. Sci. Eng. 149 (2017) 612–622.

[13] Q. Xu, M. Nakajima, S. Ichikawa, N. Nakamura, P. Roy, H. Okadome, T. Shiina, Effects of surfactant and electrolyte concentrations on bubble formation and stabilization, J. Colloid Interface Sci. 332 (2009) 208–214.

[14] S. Takagi, T. Uda, Y. Watanabe, Y. Matsumoto, Behavior of a rising bubble in water with surfactant dissolution, Trans. Jpn. Soc. Mech. Eng. Ser. B 69 (686) (2003) 2192–2199.

[15] A. Frumkin, V.G. Levich, On surfactants and interfacial motion, Zh. Fiz. Khim. 21 (1947) 1183–1204.

[16] P. Joos, G. Serrien, Adsorption kinetics of lower alkanols at the air/waterinterface: effect of structure makers and structure breakers, J. Colloid Interface Sci. 127 (1) (1989) 97–103.

[17] J. Aoki, K. Hayashi, S. Hosokawa, A. Tomiyama, Effects of surfactant on mass transfer from single carbon dioxide bubbles in vertical pipes, Chem. Eng. Tech., 38 (11) (2015) 1955–1964.

[18] S. Hosoda, S. Abe, S. Hosokawa, A. Tomiyama, Mass transfer from a bubble in a vertical pipe, Int. J. Heat Mass Transfer, 69 (2014) 215–222.

[19] K. Hayashi, S. Hosoda, G. Tryggvason, A. Tomiyama, Effects of shape oscillation on mass transfer from a Taylor bubble, Int. J. Multiph. Flow 58 (2014) 236–245.

[20] Y. Nakahara, A. Tomiyama, Shapes and rising velocities of single bubbles in vertical pipes, Trans. Jpn. Soc. Mech. Eng. B 69 (685) (2003) 2001–2009.

[21] A.C. Lochiel, P.H. Calderbank, Mass transfer in the continuous phase around axisymmetric bodies of revolution, Chemical Engineering Science, 19, (1964) 471−484.

[22] M. Filla, Gas absorption from a slug held stationary in downflowing liquid, Chem. Eng. J., 22 (1981) 213–220.